ACS APPLIED MATERIALS & INTERFACES

Research Article

www.acsami.org

Effects of Hydroxyapatite-Containing Composite Nanofibers on Osteogenesis of Mesenchymal Stem Cells In vitro and Bone Regeneration In vivo

Lan-Xin Lü,[†] Xiao-Feng Zhang,[†] Yan-Yan Wang,[†] Lazarus Ortiz,[†] Xi Mao,[‡] Zan-Li Jiang,[§] Zhong-Dang Xiao,*[,†] and Ning-Ping Huang*[,†]

[†]State Key Laboratory of Bioelectronics, School of Biological Science and Medical Engineering, Southeast University, Nanjing 210096, P. R. China

[‡]Laboratory of Developmental Genes and Human Diseases, Medical School of Southeast University, Nanjing 210009, P.R. China

[§]Department of Orthopedics, Southeast University affiliated Zhong Da Hospital, Nanjing 210009, P. R. China

Supporting Information

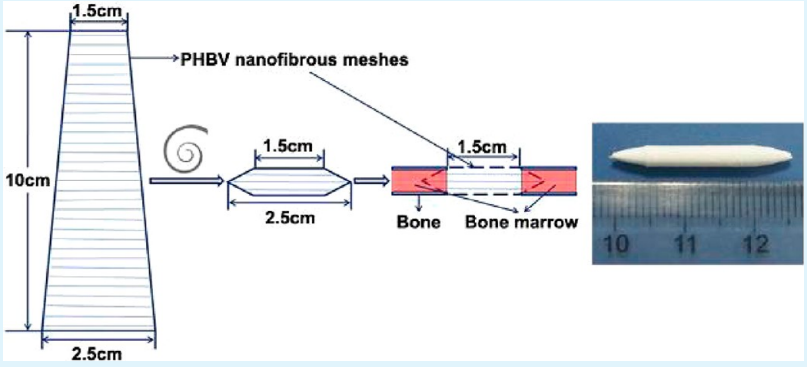

ABSTRACT: Among a variety of polymers, poly (3-hydroxybutyrate-co-3-hydroxyvalerate) (PHBV), a microbial polyester, with biodegradable, nonantigenic, and biocompatible properties, is attracting more and more attention in tissue engineering. Hydroxyapatite (HA), similar to the mineral component of natural bone, is known to be osteoconductive, nontoxic, and noninflammatory. In this study, aligned and random-oriented PHBV nanofibrous scaffolds loaded with HA nanoparticles were fabricated through electrospinning technique. Mesenchymal stem cells (MSCs) derived from rat bone marrow were used to investigate the effects of HA and orientation of fibers on cell proliferation and differentiation in vitro. Cell proliferation tested with CCK-8 assay indicated that the MSCs attached and proliferated more favorably on random-oriented PHBV nanofibrous meshes without HA. After one, two and four weeks of cell seeding, osteogenic markers including alkaline phosphate (ALP), osteocalcin (OCN), and mineralized matrix deposits were detected, respectively. The results indicated that the introduction of HA could induce MSCs to differentiate into osteoblasts. Moreover, 3D PHBV/HA scaffolds made from aligned and random-oriented nanofibers were implanted into critical-sized rabbit radius defects and exhibited significant effects on the repair of critical bone defects, implying their promising applications in bone tissue engineering.

KEYWORDS: *PHBV nanofibers, hydroxyapatite, 3D scaffolds, mesenchymal stem cells, osteogenic differentiation, bone tissue engineering*

1. INTRODUCTION

An important goal of bone tissue engineering lies in the development of biomedical scaffolds to repair large bone defects caused by trauma, tumor and infection. Tissue engineering scaffolds could connect neighboring ends of defected bones and offer three-dimensional (3D) matrix for the adhesion, proliferation, and differentiation of cells.[1] A series of biomedical materials such as bioactive inorganic substances, biodegradable polymers, and their composites have been designed into scaffolds for bone tissue engineering to study their effects on osteogenesis.[2] β-Triphosphate calcium (β-TCP) and hydroxyapatite (HA) are the most commonly used ceramic materials and have been reported to be utilized in animal models to help in the healing of many kinds of critical-sized defects.[2,3] Though these materials have the desired properties for biocompatibility and osteoconductivity, their brittle nature has restricted their utilization.[4] Many kinds of polymers such as gelatin, PLGA (poly(lactide-co-glycolide)), and PCL (poly(ε-caprolactone)), have also been used as scaffolds in bone tissue engineering.[4,5] Nowadays, composite materials composed of

Received: September 28, 2012
Accepted: December 25, 2012
Published: December 25, 2012

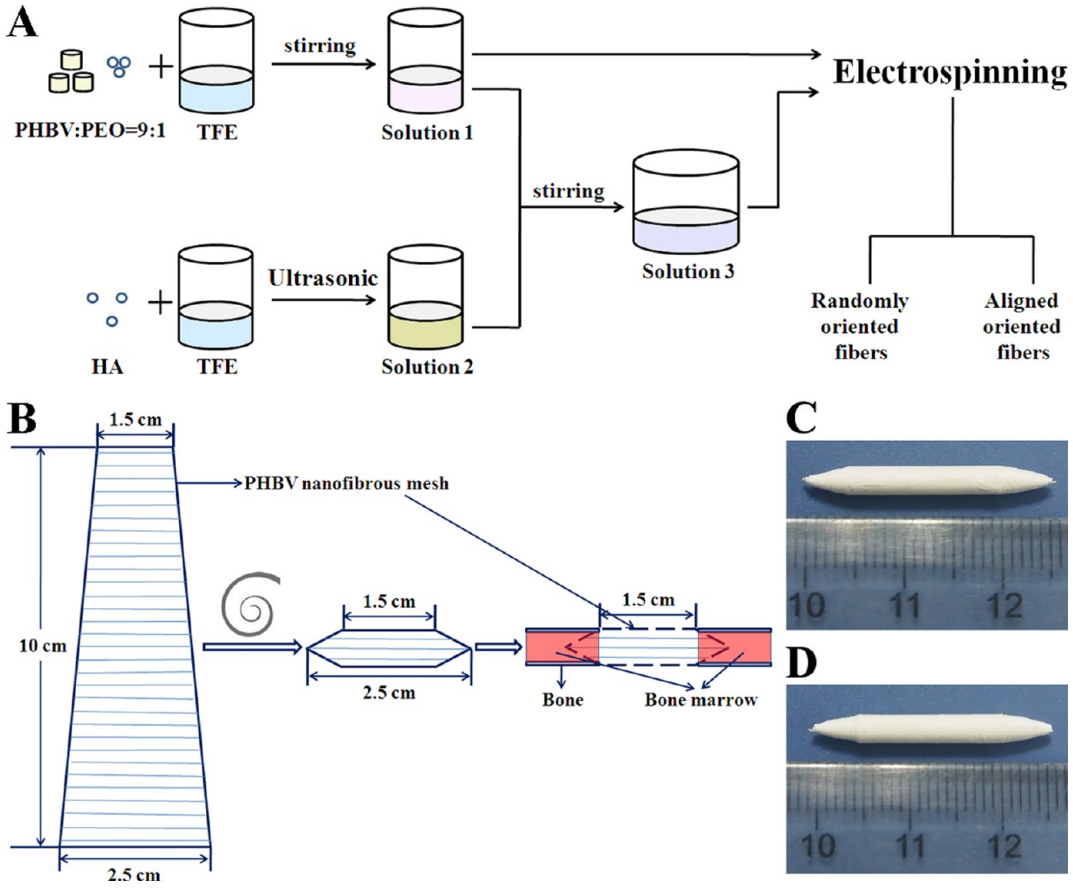

Figure 1. Schematic representation of (A) the preparation procedure of PHBV and PHBV/HA nanofibers and (B) implantable 3D PHBV/HA scaffolds. Photographic images of 3D scaffolds made from (C) random-oriented nanofibrous meshes and (D) aligned nanofibrous meshes.

inorganic substances and polymers, are being designed to improve resilience and rigidity, and have been widely investigated as scaffolds for bone tissue engineering.[6,7] It is generally accepted that among various methods for fabricating scaffolds, such as porogen leaching, phase separation/freeze-drying, and gas foaming, the electrospinning technique can generate nanoscaled fibrous scaffolds that mimic the extracellular matrix in structure as well as promote cell adhesion and proliferation.[8−12] However, nanofibrous meshes have generally been used to investigate cell behavior in vitro[7,13,14] instead of in vivo bone formation abilities.[15,16] Some researchers have studied the capability of electrospun nanofibrous scaffolds to repair critical-sized defects of flat bones (e.g., calvarium),[17−20] but no research has been reported to use these scaffolds for long bone (limbs) regeneration due to the difficulty of handling fibrous meshes for long bone repair. Therefore, how to construct 3D scaffolds from these nanofibrous meshes and use them to repair long bone defects in vivo is an important task in our study.

Another vital factor in bone tissue engineering is the cells. The bone marrow-derived mesenchymal stem cells (MSCs) are multipotent stem cells that can differentiate into a variety of cell types, including osteoblasts, chondrocytes, and neurons[21−23] in different conditions. Previous studies have proved that MSCs could be induced into osteoblasts by adding some chemical reagents into the culture media, and adjusting the topography, chemistry or stiffness of the supporting substrates.[24−29] For example, Dalby et al.[26] have demonstrated that controlled disordered nanopits could induce MSCs to produce bone mineral in vitro, in the absence of osteogenic supplements. Oh et al.[28] have reported that when cultured on nanotubular-shaped titanium oxide surfaces in the absence of osteogenic inducing media, human MSCs adhered more on smaller nanotubes (diameter of ∼30 nm), but differentiated into osteoblast-like cells on larger nanotubes (diameter in the range of 70−100 nm). Jose et al.[11] have reported that, within the osteogenic media, the random-oriented electrospun nanofibers induced osteogenesis of MSCs more effectively than flat films.

As a main inorganic component of bone, hydroxyapatite (HA) has displayed osteoconductive and "inherent" osteoinductive effect.[3] Numerous studies have confirmed that 3D porous scaffolds containing HA implanted into bone defects can induce new bone formation after several weeks of surgery.[6,9,30] The osteoinductive role of HA has been investigated by monitoring its ability to induce pluripotent MSCs to differentiate along the osteogenic pathway. Most previous research evaluated the osteoinductive ability of HA when osteogenic media or growth factors were applied.[31−33] However, few studies have investigated the individual effects of HA on osteoinductivity.[34] A recent study reported that the incorporation of either HA or TCP into the PCL nanofibrous scaffolds could regulate the osteogenic differentiation of human MSCs in total absence of osteogenic supplements.[35]

In this study, random-oriented and aligned PHBV and PHBV/HA nanofibrous scaffolds were prepared by electrospinning method. The effects of HA and orientation of fibers on MSCs proliferation and osteogenic differentiation were investigated by CCK-8 assay and by detecting the expression of

ALP, OCN and mineral deposition, respectively. Furthermore, we have processed random-oriented and aligned PHBV/HA nanofibrous meshes into rodlike scaffolds and implanted them into rabbit radius defects to investigate their effects on bone regeneration in vivo.

2. MATERIALS AND METHODS

2.1. Preparation and Characterization of PHBV-Based Scaffolds. Random-oriented and aligned PHBV and PHBV/HA fibers were fabricated via the electrospinning method;[36] the schematic procedure is shown in Figure 1A. In brief, for fabricating PHBV nanofibers, the electrospun solution was prepared as follows: PHBV (HV content 12 wt %, Sigma-Aldrich, USA) and poly (ethylene oxide) (PEO, MW ≈ 1 000 000 Da, Guoren Chemical Co., Beijing, China), with mass ratio of 9:1, were mixed in 2, 2, 2-trifluoroethanol (TFE, Darui Finechem Ltd., Shanghai, China) at a final concentration of 2 wt %, for example, 1.8 g of PHBV and 0.2 g of PEO were dissolved in 100 mL of TFE under magnetic stirring to get solution for preparing PHBV nanofibers. For fabricating PHBV/HA nanofibers, 1.8 g of PHBV and 0.2 g of PEO were dissolved in 50 mL of TFE under magnetic stirring to get Solution 1, whereas 0.2 g of hydroxyapatite (HA, diameter less than 200 nm, Sigma-Aldrich, USA) was uniformly dispersed into 50 mL of TFE in ultrasonic bath to get Solution 2. Then Solution 1 and 2 were mixed under magnetic stirring for 1 h to get solution for preparing HA-containing PHBV nanofibers. To prepare random-oriented nanofibers (NF), electrospun solution was fed into a syringe with 6# needle (inner diameter of 0.5 mm) and continually driven by an advancing pump at a speed of 5 mL per hour. The aluminum foil connected to the cathode was used as a collector for random-oriented nanofibers, whereas a roller with a rotating rate of 2500 rpm was used for collecting aligned nanofibers (A-NF). A 12 kV high DC voltage was applied between the metal needle and the collector at a certain distance. All collected fibers were dried in vacuum desiccator for 24 h at 60 °C to remove residual solvent. In order to mimic bone shape, 3D scaffolds were prepared based on random-oriented and aligned PHBV/HA fibrous meshes. For this purpose random-oriented and aligned PHBV/HA nanofibrous meshes were cut into trapezoid shapes, and those small pieces of meshes were then rolled along the longer side into a rod shape as shown in Figure.1B. Before use, all scaffolds were sterilized by autoclave at 120 °C for 20 min.

The morphology of electrospun nanofibers was observed by scanning electron microscope (SEM, ultra plus Zeiss, Germany). The average diameter of fibers was determined by measuring diameters of 100 nanofibers in SEM images using the ImageJ software. HA particles dispersed inside fibers were observed by transmission electron microscope (TEM, Tecnai G2 S-TWIN, The Netherlands).

2.2. Isolation and Identification of MSCs. MSCs from rat bone marrow were extracted as has been described previously.[36,37] Briefly, the tibias and femurs from 4-week-old Sprague−Dawley rats were dissected. Both ends of the bones were cut down along the epiphysis, then marrow was flushed with 10 mL of cell culture medium consisting of α-minimal essential medium (α-MEM, Thermo Scientific HyClone, USA) supplemented with 10% fetal bovine serum (FBS, Thermo Scientific HyClone, USA) and 1% penicillin/streptomycin antibiotics (Gibco, USA) contained in one-off syringe with steel needle. To obtain MSCs, bone marrow cells were transferred into a culture flask and incubated at 37 °C with 5% CO_2. The medium was replaced every 3 days and most nonadherent cells were removed. After 8 to 10 days, when the cells reached confluence, the culture medium was discarded and cells were washed with PBS, and incubated in 0.25% trypsin (Amresco, USA) at 37 °C for 5 min. Digestion was stopped by removing trypsin and adding 3 mL of culture medium. Suspended cells were then subcultured at a 1:2 plate ratio.

Identification and characterization of MSCs was performed using standard procedures as described in detail in the Supporting Information. Analysis by flow cytometry demonstrated the cells were negative for CD11b, CD34 and CD45, and positive for CD29 and CD90 (see the Supporting Information, Figure S1). The osteogenic and adipogenic potential of the MSCs were verified using standard assays and medium supplements, and the resulting cells were characterized using Alizarin red staining and oil red staining, respectively (see the Supporting Information, Figure S2).

2.3. Behavior of MSCs on Different Nanofibrous Meshes. MSCs at the fourth or fifth passage were planted onto PHBV random-oriented and aligned nanofibers (NF and A-NF) and HA-containing PHBV NF and A-NF (HA-NF and HA-A-NF) meshes at a density of 10 000 cells/cm^2. Normal growth medium (GM), composed of α-MEM, 10% FBS, and 1% penicillin/streptomycin antibiotics, was changed every three days in the MSCs proliferation experiment. In order to investigate the osteoinductive ability of HA and the two different nanofibrous orientations, PHBV NF and A-NF meshes seeded with MSCs in GM were chosen as negative control groups, while PHBV HA-NF and HA-A-NF meshes cultured with MSCs in GM were made experimental groups. In these two groups, GM was changed every 3 days. As positive control groups, MSCs were first seeded on the surfaces of PHBV NF and A-NF in GM. After a day of culture, GM was replaced by osteogenic medium (OM), which contains low glucose DMEM (Thermo Scientific HyClone, USA) supplemented with 10% FBS, 1% penicillin/streptomycin antibiotics, 10 mmol/L glycerol phosphate disodium salt hydrate, 10 nmol/L dexamethasone, 50 μmol/L L-ascorbic acid sodium salt, 300 mg/L L-glutamine and 10 nmol/L 1α, 25-dihydroxyvitamin D_3 (the above five chemicals were purchased from Sigma-Aldrich, USA).The OM was also changed every 3 days throughout the experiment.

2.3.1. Proliferation and Morphology of MSCs. CCK-8 Test. Cell proliferation was tested by cell counting kit-8 (CCK-8, Dojindo, Japan) as previously described.[38,39] Briefly, at 1, 4, and 7 days after cell seeding, 220 μL of CCK-8 solutions at a dilution of 1:10 with MEM media were added to each sample located in each well of a 48-well plate and cultured in an incubator at 37 °C with 5% CO_2. Three hours later, 100 μL of media were transferred to each well of a 96-well plate to measure absorption value at a wavelength of 450 nm using a microplate reader (Symergy HT, BioTek, USA). The rest media with CCK-8 solution was discarded and fresh culture media was added to each sample. The experiment was repeated three times with six parallel repeats for each sample.

Morphology of MSCs. After 7 days of culture, MSCs on different surfaces of random-oriented/aligned PHBV and PHBV/HA nanofibrous meshes were gently rinsed three times with PBS buffer and fixed with 2.5% glutaraldehyde (Sigma-Aldrich, USA) for 2 h at room temperature. After fixation, the samples were rinsed again with PBS and underwent dehydration with gradient ethanol (30, 50, 70, 80, 90, 95, and 100%) for 10 min each step. The samples were then dried and examined by SEM.

2.3.2. Osteogenic Differentiation of MSCs. After 7, 14, and 28 days of cell seeding, samples were taken out from the 48-well plate. The alkaline phosphatase (ALP) activity, osteocalcin (OCN) expression and mineralized matrix deposition were detected to evaluate the osteogenic differentiation of MSCs on the different materials.

ALP Assay. Alkaline phosphatase detection kit (BCIP/NBT, 5-bromo-4-chloro-3-indolyl phosphate/p-nitroblue tetrazolium chloride, Amresco, USA) was used to determine the ALP activity. Seven days after cell seeding, the samples were fixed with 4% paraformaldehyde (Lingfeng Chemical Reagent Co., Ltd., Shanghai, China) for 30 min and rinsed three times with PBS. BCIP/NBT was then added and they were incubated for 30 min. Finally, samples were rinsed once with water and observed under a bright-field microscope.

Fluorescent Staining of OCN, Actin, and Nucleus. To stain the OCN on different fibrous meshes, we washed samples with PBS, permeabilized by 0.5% formaldehyde (Xilong Chemical Technology Co., Ltd., Shantou, China) coupled with 0.2% Triton X-100 (SunShine Biotechnology Co., Ltd., Nanjing, China) in PBS buffer at pH 7.4 for 5 min at room temperature, and then rinsed with PBS once followed by fixation in 4% formaldehyde in PBS for 20 min. After three washes with PBS, 1% bovine serum albumin (BSA, SunShine Biotechnology Co., Ltd., Nanjing, China) in PBS was used as blocking solution to prevent nonspecific binding of antibody. After three times of rinsing with PBS, samples were immersed in osteocalcin primary antibody

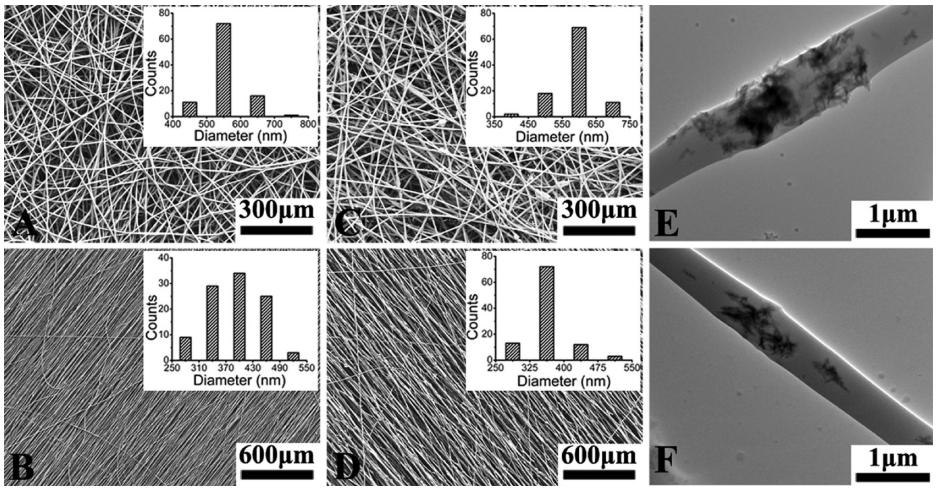

Figure 2. SEM images of (A) random-oriented PHBV nanofibers, (B) aligned PHBV nanofibers, (C) random-oriented PHBV/HA nanofibers, (D) aligned PHBV/HA nanofibers, and TEM images of (E) random-oriented PHBV/HA nanofibers, (F) aligned PHBV/HA nanofibers. The inserts show the diameter distributions of four kinds of nanofibers.

(1:100 in 1% BSA, rabbit polyclonal antibody of rat, Santa Cruz Biotechnology, USA) and incubated at 4 °C for at least 12 h. After washed with PBS, samples were incubated in secondary antibody (1:200 in 1% BSA, Alexa-Fluor 488 goat antirabbit IgG, Invitrogen, USA) for 1 h at 37 °C protected from light. Samples were washed twice and then incubated with Alexa-Fluor 633 phalloidin (Invitrogen, USA) at a dilution of 1:100 in the dark for 30 min followed by rinsing twice with PBS. Finally, to stain nucleus, samples were immersed in hoechst 33342 (Sigma, USA) at a concentration of 10 μg/mL for 30 min protected from light. All samples were embedded with neutral balsam to reduce the quenching of fluorescence.

A spinning disk confocal system (Revolution XD, Andor Technology, Northern Ireland) built on the left port of Ti-E inverted microscope (Nikon, Japan) was used to observe all samples and the confocal images were collected by an electron-multiplying CCD (EMCCD) iXon DV885 (Andor Technology).[40] 405, 491, and 640 nm solid-state lasers modulated by AOTF (acousto-optic tunable filter) were used as the illumination sources for Hoechst 33342, OCN and actin, respectively. Fluorescence emission was collected by 20× objective, passed through EM 452/45, EM 520/15 and EM 685/40 emission filters (Semrock, USA). All images were obtained with a fixed parameter of AOTF.

Real-Time PCR. After 1 and 2 weeks of culture, total RNA of the cells on nanofibrous meshes was extracted by Trizol reagent (Invitrogen, USA). The quality of RNA was detected by spectrophotometric (BioTek, USA). The first strand synthesis of cDNA was performed using equal amount of RNA samples (2 μL), according to M-MLV reserve transcriptase instructions (Promega, USA). Real time PCR was used to analyze gene expression levels of ALP and OCN. GAPDH was employed as housekeeping gene. Primer sequences we used were listed in Table S1 (see the Supporting Information). PCR reactions were performed using SYBR Premix Ex Taq (TaKaRa, Dalian, China) in a total volume of 20 μL (1.5 μL cDNA samples). Real time PCR was carried out by using ABI 7500 real time PCR system (Application Biosystems, USA). Relative expression of ALP and OCN gene was calculated by the comparative $2^{-\Delta\Delta Ct}$ method,[41] where $\Delta\Delta Ct = (Ct_{Target} - Ct_{GAPDH}) - (Ct_{Control} - Ct_{GAPDH})$. Each sample was assessed at least in triplicate.

Alizarin Red Staining for Mineralization. In order to stain the calcium mineralization on different meshes, cells were fixed with 70% ethanol for 1 h at room temperature. After washed once with water, samples were immersed in 40 mM Alizarin red S (ARS, Sigma, USA) for 20 min and then washed five times with water. All samples were observed under bright field microscope. The reaction products of ARS and calcium mineralization on different samples were dissolved with 10% cetylpyridinium chloride in water for 15 min at 37 °C. HA-NF and HA-A-NF meshes (without seeding cells) stained with ARS were chosen as control. Absorbance of ARS extracts was measured at 560 nm with a microplate reader (Symergy HT, BioTek, USA).

2.4. Animal Model and In vivo Study. Twenty-four three-month-old New Zealand white rabbits weighing 2.0−2.5 kg were used to create bone defect model. All animals were kept in the Animal Center of Southeast University and divided into three groups stochastically. The experiment protocol was approved by the Animal Center of Southeast University, in accordance with the institutional guidelines for care and use of laboratory animals. The experimental procedures were as follows: animals were anesthetized by injection of 30 mg/kg sodium pentobarbital (Merck, Germany) and critical-sized defects with lengths of 1.5 cm were created in the middle part of left radius.[42−45] After the debris at defect sites was washed away by sterile physiological saline solution, defects were filled with 3D PHBV HA-NF or HA-A-NF scaffolds (preparation procedures see Figure 1 and Section 2.1), or commercial artificial bones (calcium sulfate bone graft substitutes, cylindrical particles with the diameter of ∼4.9 mm and height of ∼3.3 mm, the name of the manufacturer is omitted.) as controls. The muscle and skin were then sutured separately with 4−0 sutures. After the surgery, all rabbits were raised in the same environment as before and were given muscle injection of penicillin with a dose of 400 000 units (Lu kang pharmaceutical Co. Ltd., Shandong, China) for 3 days.

2.4.1. X-ray Radiograph. A digital radiography X-ray system (DR, IDC Canada) was used to evaluate the mineralization and osteogenisis of rabbit radius defects after 1, 4, 8, and 12 weeks of surgery.

2.4.2. Histological Analysis. The samples were fixed with 4% paraformaldehyde, decalcified in 0.1 M HCl, embedded in O.C.T. Compound (Tissue-Tek, SAKURA, USA), and frozen in −80 °C for 3 h. Sections with 15 μm thickness were made by Shandon Cryotome PSE (Thermo, USA) and stained with Hematoxylin and Eosin Staining Kit (HE, Beyotime, China). The area of newly formed bone was examined under light microscopy.

2.4.3. Mechanical Test. Animals were sacrificed by anesthetic overdose 16 weeks after implantation. The repaired left radii after implantation of 3D PHBV HA-NF or HA-A-NF scaffolds were taken out for testing of their mechanical properties. The right normal radius of each rabbit was taken out and tested as a control.

2.4.4. SEM Images of New Bones. SEM was used to investigate the morphology of new-formed bones which were acquired from repaired radii after implantation of PHBV HA-NF or HA-A-NF scaffolds for 16 weeks. The new bones taken out from rabbit were fixed with 4% paraformaldehyde for 24 h at room temperature, and then dehydrated with gradient ethanol (30, 50, 70, 90, and 100%) for 30 min each step.

2.5. Statistical Analysis. The in vitro studies were repeated for three times using different rats as the source of MSCs. One-way analysis of variance (ANOVA) was used to compare the means among six repeated samples and *t*-test was performed to analyze the difference between two groups. A value of $P < 0.05$ was considered to be statistically significant.

3. RESULTS

3.1. Fabrication of Nanofibers and 3D Scaffolds. Electrospinning method was used to create random-oriented/aligned PHBV and PHBV/HA nanofibers; Figure 1 shows the preparation procedures of the electrospun solutions, nanofibers (Figure 1A), implantable 3D scaffolds (Figure 1B), and the photographic images of 3D scaffolds made from random-oriented (Figure 1C) and aligned (Figure 1D) nanofibrous meshes. The 3D scaffold was layered into hollow tubes with inner diameter of 0.5 mm and outside diameter of 3 mm. Figure 2A–D show the morphologies of NF, A-NF, HA-NF, and HA-A-NF observed under SEM with the diameter of 554 ± 52 nm, 381 ± 65 nm, 584 ± 52 nm, and 369 ± 60 nm, respectively. The insets show the diameter distribution of each kind of fiber mesh, from which it can be seen that fibers are uniform in diameter. Most aligned PHBV or PHBV/HA fibers are oriented parallel to each other. The SEM images indicate that the introduction of HA does not influence the continuity of nanofibers. However, some HA aggregates are found at the surfaces or the interconnection points of randomly oriented nanofibers (Figure 2C), which may cause the slight increase in the diameter of HA-NF fibers. Some are distributed inside the nanofibers as indicated in TEM images (Figure 2E, F).

3.2. Proliferation and Differentiation of MSCs on Nanofibrous Meshes. The proliferation of MSCs on nanofibrous meshes was tested by CCK-8 assay at 1, 4, and 7 days (Figure 3) and the morphology of MSCs was observed by SEM (Figure 4). From the proliferation test it can be found that cell attachment on PHBV NF surfaces was similar to that on PHBV HA-NF surfaces on the first day after cell seeding, while more cells were detected on PHBV A-NF surfaces than on PHBV HA-A-NF surfaces ($P < 0.05$). Comparing the cell proliferation on surfaces of NF and A-NF with that on HA-NF and HA-A-NF, respectively, at 4 and 7 days after cell seeding, it is apparent that the introduction of HA slowed down cell proliferation ($P < 0.05$). SEM images of MSCs after 7 days of culture on these four different fibrous meshes also indicate similar cell proliferation tendency (Figure 4A, C, E, and G). In addition, magnified SEM images show that MSCs could spread along the nanofibrous meshes. On the aligned A-NF and HA-A-NF surfaces, MSCs were elongated along the nanofibers (Figure 4D, H). On the random-oriented NF and HA-NF surfaces, MSCs spread in random directions (Figure 4B, F). Cell filopodia could be observed extending along the nanofibers on all types of fibrous meshes.

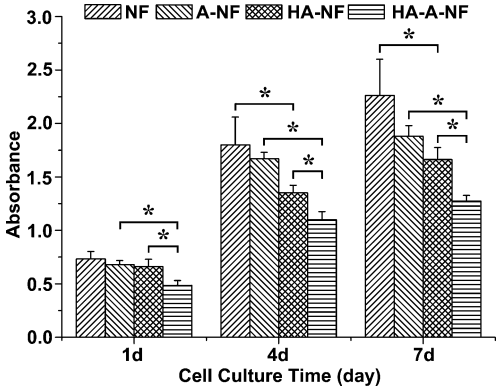

Figure 3. Viability of MSCs on different PHBV nanofibrous meshes. NF, PHBV nanofibers; A-NF, aligned PHBV nanofibers; HA-NF, PHBV/HA nanofibers; HA-A-NF, aligned PHBV/HA nanofibers. Six parallel repeats were tested for each sample; the bar indicates standard deviation. (*): $P < 0.05$.

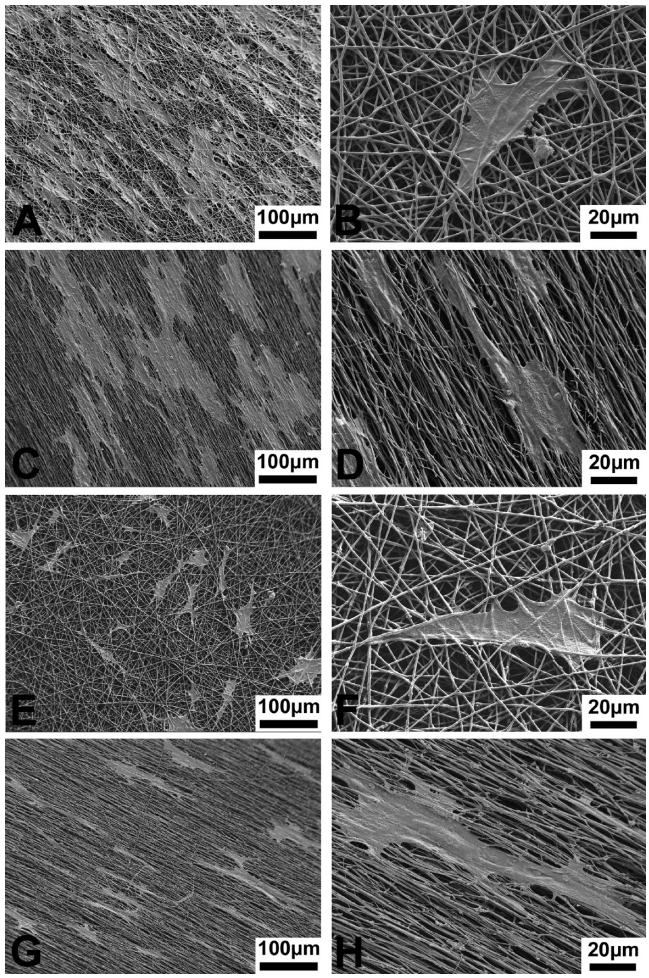

Figure 4. SEM images of MSCs after 7 days of culture on (A, B) NF, (C, D) A-NF, (E, F) HA-NF, and (G, H) HA-A-NF.

ALP, OCN, and calcium deposits in MSCs were detected using chromogenic substrate kit, immunofluorescence staining, and chemistry staining, respectively; this, in order to qualitatively evaluate osteogenisis. The ALP activity was tested by BCIP/NBT kit after 7 days of cell seeding. The stained results were observed by microscope and captured by Canon camera. Figure 5 shows the ALP staining images of MSCs on different nanofibrous meshes in GM or in OM (Figure 5A–F). The inserts show the digital images of the whole ALP-stained mesh surfaces. It is clear that in GM, MSCs express significantly higher ALP activity on HA-containing PHBV nanofibrous meshes (both aligned and random-oriented, Figure 5B, E) than on nanofibrous meshes without HA (Figure 5A, D). The ALP activity expressed by MSCs on HA-NF and HA-A-NF meshes in GM is even higher than that of NF and A-NF meshes in OM (Figure 5C, F). However, no significant difference on ALP

dx.doi.org/10.1021/am302146w | ACS Appl. Mater. Interfaces 2013, 5, 319–330

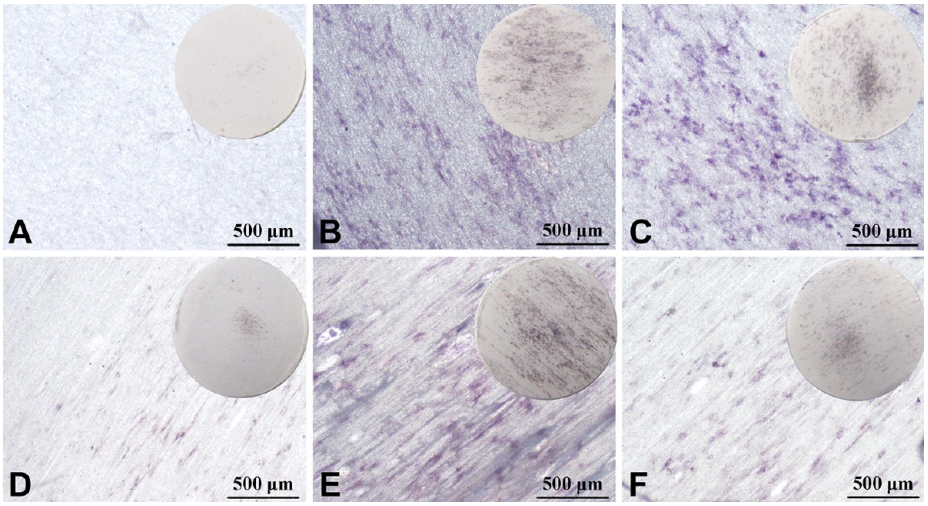

Figure 5. ALP staining of MSCs cultured on different PHBV nanofibrous meshes in different media for 7 days. The inserts show macroscopic images. (A, D) On NF and A-NF in GM, (B, E) on HA-NF and HA-A-NF in GM, (C, F) on NF and A-NF in OM.

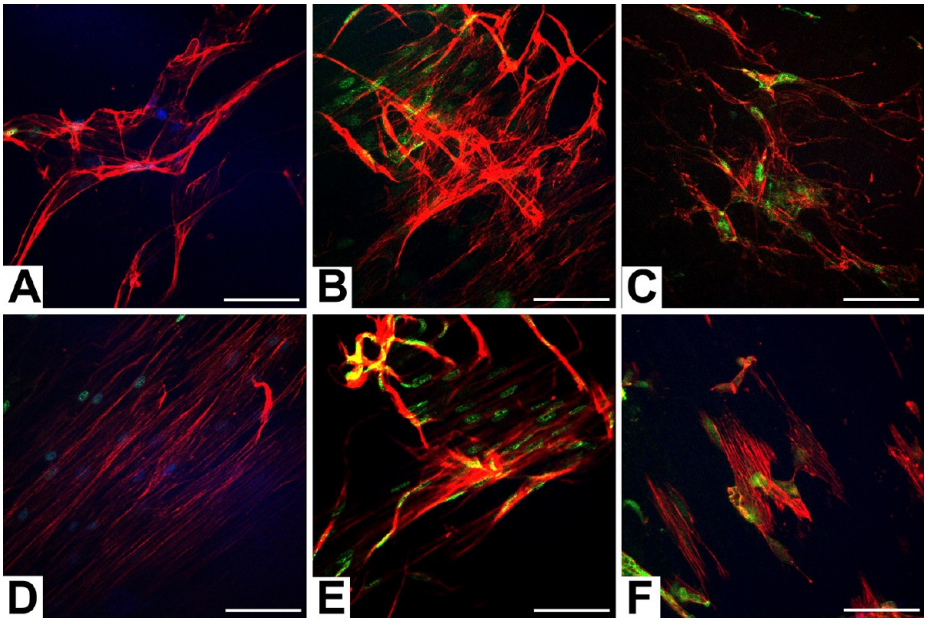

Figure 6. Immunofluorescent staining of OCN 14 days after MSCs were cultured on different PHBV nanofibrous meshes in different media. (A, D) On NF and A-NF in GM, (B, E) on HA-NF and HA-A-NF in GM, (C, F) on NF and A-NF in OM. Red, actin; blue, nucleus; green, OCN. Scale bar: 100 μm.

expression is observed between HA-NF and HA-A-NF meshes (Figure 5B, E).

Figure 6 shows the immunofluorescence images of OCN 14 days after MSCs seeding on different meshes. Very little green fluorescence is observed on NF and A-NF surfaces when seeded MSCs were cultured in GM (Figure 6A, D). Upon the addition of HA in scaffolds, more OCN is expressed on HA-NF and HA-A-NF (Figure 6B, E); the OCN expression level is even higher than that on NF and A-NF when seeded MSCs were cultured in OM (Figure 6C, F). The above results are in good agreement with the results from ALP expression.

To further support the staining results described above, we also studied ALP and OCN gene expressions by quantitative real time PCR analysis after 7 and 14 days of cell culture, with the analysis data shown in Figure 7. Compared to negative control (NF in GM), the levels of ALP and OCN gene expression were up-regulated when MSCs cultured on HA-NF in GM and on NF in OM (Figure 7A and B). The expression level of ALP on HA-NF in GM was even higher than that on NF in OM at both tested time points (Figure 7A), whereas the OCN expression level on HA-NF in GM was lower at day 7 but higher at day 14 than that on NF in OM ($P < 0.05$) (Figure 7B). Figure 7C–E show both ALP and OCN levels when MSCs cultured on HA-NF in GM, NF in OM and NF in GM compared to those on HA-A-NF in GM, A-NF in OM and A-NF in GM, respectively. From Figure 7C, it can be found that the expression levels of ALP and OCN of cells cultured on HA-NF were much higher than those on HA-A-NF in GM (fold changes >2). While compared to A-NF, the expression levels of ALP and OCN of cells cultured on NF were up-regulated slightly both in OM and GM (fold changes <2) (Figure 7D, E).

Levels of mineral deposition were detected by staining with ARS; micrographs and quantitative results are shown in Figure 8. From the bright-field pictures, we found that there was little

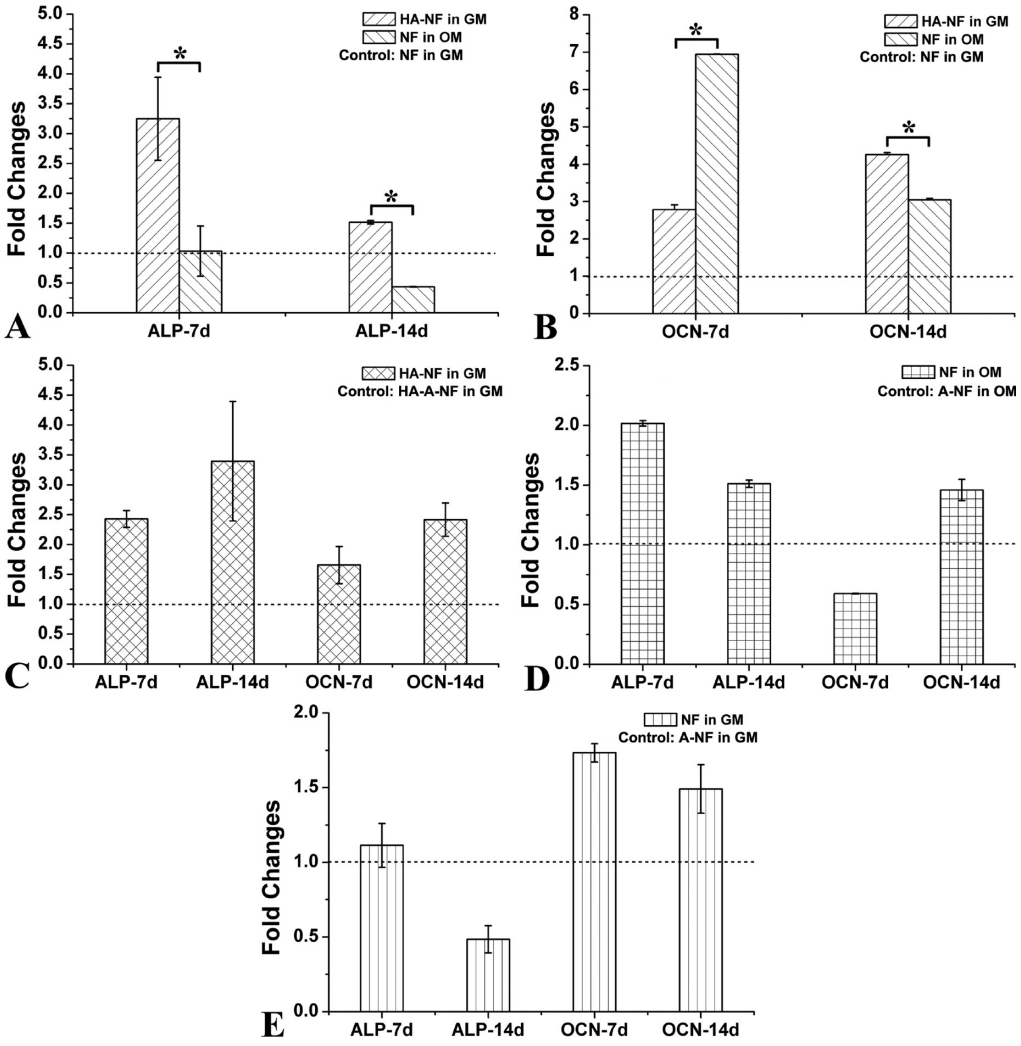

Figure 7. Quantitative real time PCR gene expression analysis of osteoblast-related genes. (A, B) ALP and OCN expression levels for MSCs cultured on HA-NF in GM and NF in OM compared to NF in GM at day 7 and 14, (C–E) ALP and OCN expression levels for MSCs cultured on HA-NF in GM, NF in OM, and NF in GM compared to HA-A-NF in GM, A-NF in OM, and A-NF in GM, respectively. Results are reported as mean ± standard deviation.

mineral deposits on NF and A-NF surfaces in GM (Figure 8A, D), whereas many more calcium deposits were stained by ARS on NF and A-NF surfaces in OM (Figure 8C, F). With the introduction of HA, HA-NF, and HA-A-NF meshes in GM were optimal for inducing the differentiation of MSCs into osteoblasts (Figure 8B and E). Figure 8G shows the quantitative analysis of mineral deposits by subtracting the background from fibrous meshes (without seeding cells). The results are consistent with the staining micrographs. It is clear that more mineral deposits are obtained in both experimental group (HA-NF and HA-A-NF in GM) and positive control group (NF and A-NF in OM) than in negative control group (NF and A-NF in GM). The mineral deposits on HA-NF and HA-A-NF meshes in GM are even higher than those on NF and A-NF meshes in OM. However, no significant difference has been observed between random-oriented and aligned nanofibrous meshes in all three groups.

3.3. Repair of Critical-Sized Radius Defects. Figure 9 shows radiographs of rabbit radius defects implanted with 3D HA-NF scaffolds, 3D HA-A-NF scaffolds or commercial artificial bones (as controls) at 1, 4, 8, and 12 weeks post surgery.

At 1 week post surgery, the implanted 3D HA-NF and HA-A-NF scaffolds are not visible at bone defect sites in the X-ray radiographs (Figure 9A-1 and B-1) because of the relative low molecular mass of materials, which makes it easy for new-formed bone to be distinguished. Only a little bone formation at the left end of bone defect can be observed in HA-A-NF group (Figure 9B-1), while more amount of new-formed bone is observed in HA-NF group (Figure 9A-1). In the control group, the implantation of commercial artificial bones which are mainly composed of calcium sulfate can be clearly seen in the X-ray radiograph (Figure 9C-1).

At 4 weeks post surgery, in both the groups of HA-NF and HA-A-NF, significant new-bone formation occurred at both ends of the bone defects with good connection to the neighboring host bones (Figure 9A-2 and B-2). However, in the group of commercial artificial bones, the implanted materials were dispersed totally and little mineralization appeared (Figure 9C-2).

At 8 weeks post surgery, the densities of mineralization along implanted scaffolds in the repaired areas continuously increased in the groups of HA-NF and HA-A-NF (Figure 9A-3 and 9B-3). In the control group, new-bone formation appeared at both

dx.doi.org/10.1021/am302146w | ACS Appl. Mater. Interfaces 2013, 5, 319–330

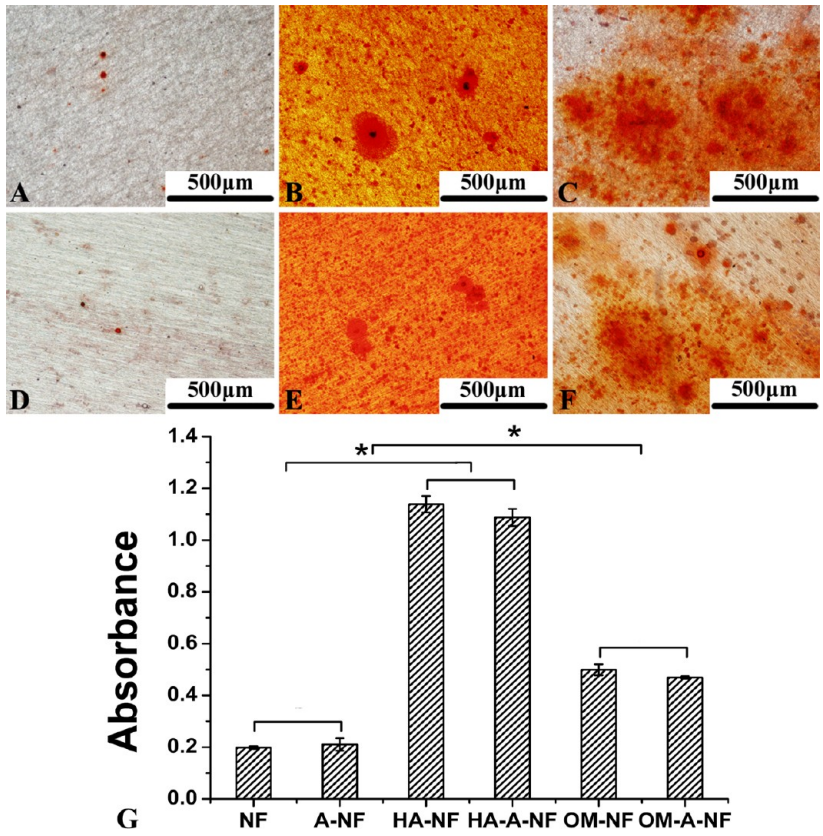

Figure 8. Mineral deposition staining of MSCs cultured on different PHBV nanofibrous meshes in different media for 28 days. (A, D) on NF and A-NF in GM, (B, E) on HA-NF and HA-A-NF in GM, (C, F) on NF and A-NF in OM, (G) Quantification of mineral deposition by detecting absorbance of ARS extracts. Results are reported as mean ± standard deviation. (*): $P < 0.05$.

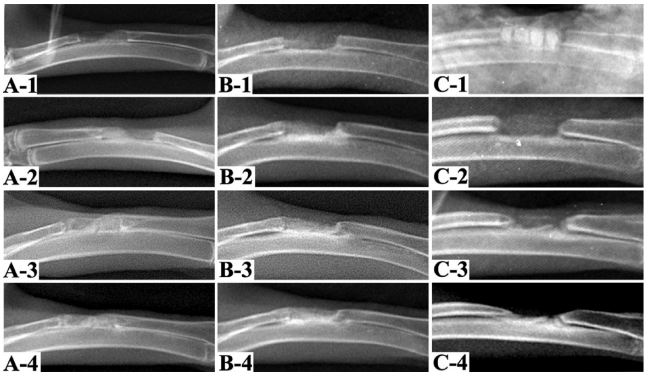

Figure 9. X-ray radiographs of rabbit radii defects implanted with the 3D scaffolds of HA-NF (A-1−A-4), HA-A-NF (B-1−B-4), and commercial artificial bones (C-1−C-4) after 1, 4, 8, and 12 weeks of surgery.

ends of defected radius and medullary cavity of bone began to be blocked (Figure 9C-3).

At 12 weeks post surgery, the bone defects were completely filled with new cortical bone in the groups of HA-NF and HA-A-NF (Figure 9A-4 and B-4). However, medullary cavity of bone was blocked completely in the control group (Figure 9C-4).

Figure.10 shows typical histological sections of 3D HA-A-NF scaffolds after 16 weeks of implantation. It can be seen that the new-formed bones (blue arrows) have grown into the cavity between undegraded nanofiber layers (green arrows).

Sixteen weeks later, the experimental left rabbit radii, which had undergone implantation, were taken out for mechanical properties testing. The right normal radii of rabbits were taken as controls. Figure 11 shows the stress−strain curves obtained from the repaired bones from HA-NF and HA-A-NF groups. It can be found that both strain values of the two experimental groups were less than seventy percent of normal groups, which indicated that the amount of collagen in the regenerated radius was less than that in normal bones.[46,47] The elasticity modulus could be obtained by calculating the ratio of stress value to strain value according to the stress−strain curve. The elasticity modulus of experimental group of HA-NF (E_B = 361.83 ± 23.88 MPa) was smaller than that of normal group ($E_{B'}$ = 432.82 ± 70.96 MPa), while the data in the experimental group of HA-A-NF (E_A = 471.02 ± 33.42 MPa) was similar to the normal group ($E_{A'}$ = 438.28 ± 29.99 MPa).

SEM was used to investigate the inner structure of new-formed bones. Figure 12A, B showed the cross-section of a little piece of new bone obtained from HA-NF group and HA-A-NF group, respectively. The magnified images (Figure 12C, D) indicate new collagen fibers and remaining scaffold materials as pointed by white arrows and black arrows, respectively. Meanwhile, massive deposited minerals can be found inside the HA-NF and HA-A-NF scaffolds. Large amounts of calcium and phosphorus were detected in the new-formed bones by energy dispersive spectrometer (EDS, Figure 12B inset)

4. DISCUSSION

In our previous studies, the condition for fabricating PHBV electrospun fibers has been optimized.[36] PEO was introduced

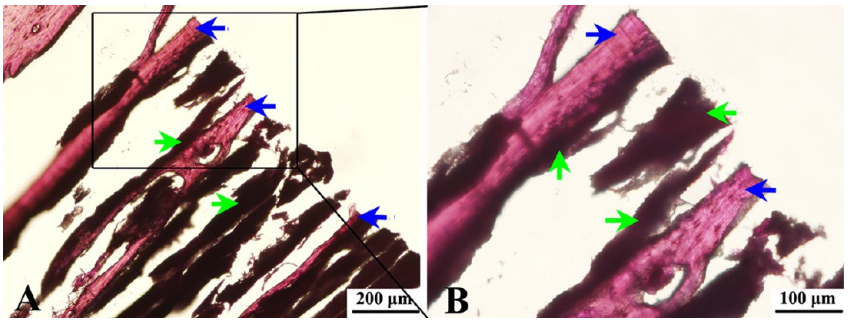

Figure 10. Histological sections of rabbit radius defects implanted with 3D HA-A-NF scaffolds after 16 weeks of implantation. (B) Amplification of the square area in A. Blue arrows, newly formed bones; green arrows, the remaining undegraded materials.

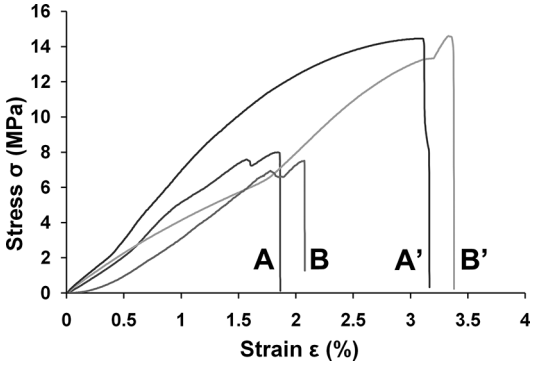

Figure 11. Mechanical tests of the repaired rabbit radii (left radius) 16 weeks after implantation of (A) 3D HA-A-NF scaffolds and (B) 3D HA-NF scaffolds. (A′) and (B′) Control tests performed on the normal radii (right radius) of rabbits implanted with HA-A-NF and HA-NF scaffolds, respectively.

to improve the processability of PHBV fibers and reduce the PHBV concentration required for obtaining continuous fibers. In this study, a novel kind of 3D PHBV/HA scaffold was further fabricated by electrospinning technique and applied in bone tissue engineering. Electrospun nanofibrous scaffolds could provide a suitable surface for cell attachment and proliferation by mimicking the structure of natural extracellular matrices (ECMs). The SEM and TEM images of HA-containing nanofibers indicated that HA nanoparticles disperse both inside and outside the fibers. The diameter of aligned nanofibers was smaller than that of random-oriented nanofibers, likely due to the stretching force induced from rotating rollers. As the mineral component of natural bone, HA is considered osteoconductive and bioactive, allowing new bone formation. It has been widely employed as bone substitute in the clinical arena.[48] The effect of loaded HA on attachment and proliferation of cells (e.g., osteoblasts, MC3T3-E1, MSCs) has also been investigated previously.[14,49−53] It has been proposed that cells were sensitive to the composition and properties of scaffolds, such as the concentration and size of loaded HA particles, surface roughness and porosity of the composites. In this study, the effect of HA-loaded PHBV nanofibers on the attachment and proliferation of MSCs was studied using CCK-8 assay and SEM. As shown in Figure 3, the MSCs keep

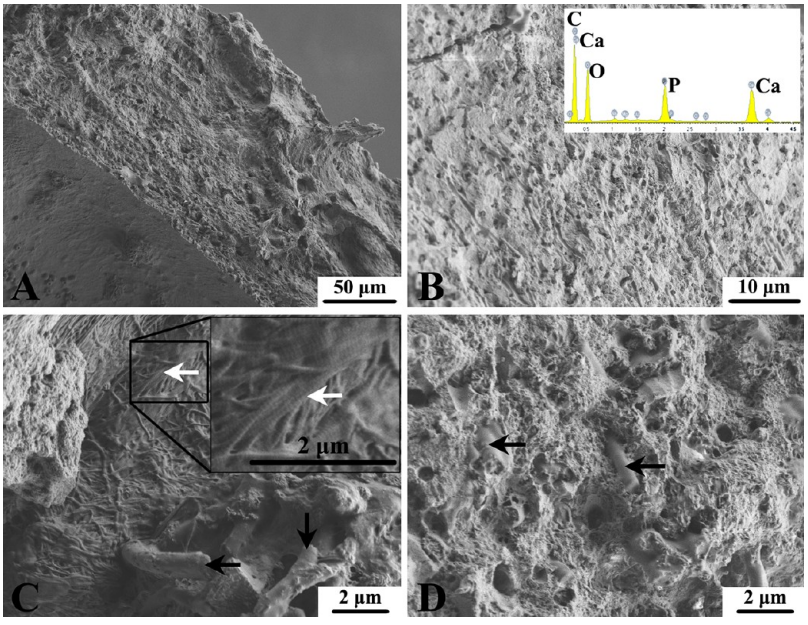

Figure 12. SEM images of newly formed bones. (A) A piece of new bone at bone defect sites after implantation with 3D HA-NF scaffolds. (B) A piece of new bone at bone defect sites after implantation with 3D HA-A-NF scaffolds, inset: EDS spectrum. (C) Magnified area of A, inset: amplification of the square area in C. (D) magnified area of B. White arrows indicate the new collagen fibers and black arrows indicate the remaining undegraded materials.

dx.doi.org/10.1021/am302146w | ACS Appl. Mater. Interfaces 2013, 5, 319−330

proliferating on all sample surfaces within the 7 culture days after seeding. However, the introduction of HA to PHBV nanofibers significantly slows down the proliferation rate of MSCs compared with pure PHBV nanofibers, which is likely due to the differentiation of MSCs toward osteoblasts induced by HA as we can see from the following ALP staining and OCN immunostainning (Figures 5 and 6).

HA is considered an osteoconductive and "inherent" osteoinductive material. This is based on numerous studies which proved the capability of HA to promote new bone formation in vivo.[6,9,30,54] It has been recently reported that HA is also osteoinductive in the absence of osteogenic factors.[35] In this study, the osteoinductive property of HA was also found by in vitro investigating the osteogenic differentiation of MSCs on various nanofibrous scaffolds without adding any osteogenic factors. At different stages of the differentiation process, the expressions of ALP, OCN, and mineral deposits were qualitatively and quantitatively detected. ALP is considered as an early differentiation marker because ALP expression level is associated with the activity of osteoblasts and new bone formation. The higher ALP expression was found when MSCs were cultured on PHBV/HA scaffolds in GM or on PHBV scaffolds in OM compared to that on PHBV scaffolds in GM regardless of the fiber orientation. The fact that the ALP expression level on PHBV/HA scaffolds in GM is higher than that on PHBV scaffolds in OM (Figure 7A) indicates that the introduction of HA has a similar effect as OM on stimulating the osteogenic differentiation of MSCs in early stage. OCN, secreted by mature osteoblasts, was also detected on those scaffolds seeded with MSCs in different culture media. The positive OCN expressions on PHBV/HA scaffolds in GM and on PHBV scaffolds in OM demonstrate that the scaffolds loaded with HA nanoparticles have similar osteoinductivity to the OM (Figure 7B). Furthermore, calcium nodule creation was detected by ARS staining and hence is in good agreement with OCN expression results. The mineral deposits on PHBV scaffolds in OM were less than those on PHBV/HA scaffolds in GM no matter what the fiber orientation was (Figure 8G). The osteogenic differentiation of MSCs was not significantly affected by fiber orientations when HA was absent according to our study (Figure 7D, E, Figure 8G). This phenomenon has also been observed in a recent study by Wei et al.[49] However, Yin et al. previously found that when cultured on aligned nanofibers, human tendon stem/progenitor cells (hTSPCs) had lower expression of osteogenic markers but higher tendon-specific genes expression than those on randomly oriented nanofibers.[55] These disparities may attribute to the different types of stem cells. Additionally, in our study, when HA was introduced, the expressions of osteogenic genes were much higher on random-oriented nanofiber surfaces than those on aligned nanofiber surfaces, which indicated that the HA-containing random-oriented nanofibers were favorable for early stage osteogenic differentiation of MSCs in vitro. However, no significant difference has been observed in the amount of mineral deposits between HA-NF and HA-A-NF meshes in GM.

A critical-sized bone defect model was used to study the bone repair capability of PHBV/HA 3D scaffolds compared with a commercial artificial bone product, which is a calcium sulfate bone graft substitute. From the radiographic results it can be seen that the critical-sized rabbit radius defect (1.5 cm in length) was repaired completely with implantation of 3D scaffolds, based on either random-oriented or aligned PHBV/HA nanofibers, indicating the excellent bone regeneration effects of our 3D PHBV/HA scaffolds. Bone mechanical property is an important criterion for the evaluation of bone fracture healing. Compared with 3D PHBV HA-NF scaffolds, the elasticity modulus of the repaired radius where 3D PHBV HA-A-NF scaffolds were implanted was much closer to the value of the normal radius. Based on results of cell differentiation and in vivo animal tests, we do not observe considerable differences between the effects of PHBV HA-NF and HA-A-NF on MSCs differentiation or bone repair. However, if considering the differences in the mechanical properties of healed bones caused by different fiber orientations, we propose that PHBV HA-A-NF scaffolds are more suitable for bone tissue engineering. In this study, the differences in diameter were not investigated because only comparing random and aligned NFs with the same averaged diameter could show any significant differences. The superiority of our PHBV/HA scaffolds to the commercial artificial bones used as controls in our experiments or to some other 3D porous scaffolds was shown as following: (1) The two ends of the 3D nanofibrous scaffolds were designed in the shape of a cone (Figure 1B–D), which makes it easier to insert the scaffolds into the cavity of impaired radius with tight connection, and thus facilitates bone healing. (2) The cylindrical scaffolds bridge the bone defect and guide new bone regeneration from the host bone along implant interfaces (Figure 10). The hollow structure allows bone marrow to fill the interior of scaffolds and MSCs could be recruited into scaffolds. (3) Each layer of these coiled cylindrical scaffolds has nanofibrous surface, which is desirable for MSCs adhesion and proliferation. The dispersed HA nanoparticles play an important role in osteoinduction of MSCs.

The current 3D PHBV/HA scaffolds have exhibited good capacity for repairing rabbit bone defects. However, these scaffolds can be further improved in terms of the degradability. Twelve weeks after implantation, the rabbit radii with scaffolds were taken out and the scaffold pieces could still be found inside the deposited minerals, which may hinder the formation and maturation of new bones at the late stage of bone healing. Therefore, our next work will aim to optimize the material composition and obtain PHBV/HA scaffolds with favorable degradation rate.

5. CONCLUSION

In this study, we prepared PHBV and PHBV/HA fibrous scaffolds with different orientations. The growth behavior of MSCs on the PHBV and PHBV/HA nanofibrous meshes (random-oriented and aligned) indicated that MSCs attached and proliferated more favorably on random-oriented PHBV nanofibrous meshes without HA. The study shows that the introduction of HA could induce the osteogenic differentiation of MSCs. The orientation of nanofibers showed a distinct effect on cell morphology. Compared to HA-containing aligned nanofibers, the HA-containing random-oriented nanofibers were favorable for early stage osteogenic differentiation of MSCs in vitro, but there is no obvious difference between them in the mineral deposition. In vivo animal tests indicated that 3D PHBV nanofibrous scaffolds containing HA nanoparticles had significant effects on the repair of critical-sized rabbit bone defects compared with calcium sulfate-based commercial artificial bones. The mechanical properties of repaired bones after implantation of 3D PHBV/HA scaffolds with different fiber orientations indicated that PHBV/HA scaffolds composed

of aligned nanofibers are more suitable for bone tissue engineering compared to those composed of random-oriented nanofibers.

■ ASSOCIATED CONTENT

Supporting Information

Identification and characterization of mesenchymal stem cells (MSCs) isolated from rat bone marrow and the primer sequences used in real time PCR. This material is available free of charge via the Internet at http://pubs.acs.org.

■ AUTHOR INFORMATION

Corresponding Author

*E-mail: nphuang@seu.edu.cn (N.-P.H.); zdxiao@seu.edu.cn (Z.-D.X.). Tel.: +86 25 8379 0820 (N.-P.H.); +86 25 8379 0820 (Z.-D.X.). Fax: +86 25 8379 5635 (N.-P.H.); +86 25 8379 5635 (Z.-D.X.).

Notes

The authors declare no competing financial interest.

■ ACKNOWLEDGMENTS

This work was supported by the National Science Foundation of China (No. 30870626, 61071047), the International Cooperation Program awarded by the Ministry of Science and Technology of China (2008DFA51180), the Program Granted for Scientific Innovation Research of College Graduate in Jiangsu province (CXZZ_0170), and the National Program on Key Basic Research Project ('973' Program, 2013CB932900).

■ REFERENCES

(1) Caplan, A. I. *Tissue Eng.* **2005**, *11*, 1198−1211.
(2) Szpalski, C.; Wetterau, M.; Barr, J.; Warren, S. M. *Tissue Eng., Part B* **2012**, *18*, 246−257.
(3) LeGeros, R. Z. *Chem. Rev.* **2008**, *108*, 4742−4753.
(4) Stevens, M. M. *Mater. Today* **2008**, *11*, 18−25.
(5) Molera, J. G.; Mendez, J. A.; Roman, J. S. *Curr. Pharm. Des.* **2012**, *18*, 2536−2557.
(6) Kaito, T.; Myoui, A.; Takaoka, K.; Saito, N.; Nishikawa, M.; Tamai, N.; Ohgushi, H.; Yoshikawa, H. *Biomaterials* **2005**, *26*, 73−79.
(7) Prabhakaran, M. P.; Venugopal, J.; Ramakrishna, S. *Acta Biomater.* **2009**, *5*, 2884−2893.
(8) Liu, G.; Zhao, L.; Cui, L.; Liu, W.; Cao, Y. *Biomed Mater* **2007**, *2*, 78−86.
(9) Zhang, P.; Hong, Z.; Yu, T.; Chen, X.; Jing, X. *Biomaterials* **2009**, *30*, 58−70.
(10) Zhang, Y.; Wu, C.; Friis, T.; Xiao, Y. *Biomaterials* **2010**, *31*, 2848−2856.
(11) Jose, M. V.; Thomas, V.; Xu, Y. Y.; Bellis, S.; Nyairo, E.; Dean, D. *Macromol. Biosci.* **2010**, *10*, 433−444.
(12) Hoshi, R. A.; Behl, S.; Ameer, G. A. *Adv. Mater.* **2009**, *21*, 188−192.
(13) Supaphol, P.; Chuenjitkuntaworn, B.; Pavasant, P.; Damrongsri, D. *Polym. Int.* **2010**, *59*, 227−235.
(14) Ngiam, M.; Liao, S.; Patil, A. J.; Cheng, Z.; Chan, C. K.; Ramakrishna, S. *Bone* **2009**, *45*, 4−16.
(15) Srouji, S.; Ben-David, D.; Lotan, R.; Livne, E.; Avrahami, R.; Zussman, E. *Tissue Eng., Part A* **2011**, *17*, 269−277.
(16) Kim, J. H.; Kim, M. K.; Park, J. H.; Won, J. E.; Kim, T. H.; Kim, H. W. *In Vivo* **2011**, *25*, 589−595.
(17) Dinaryand, P.; Seyedjafari, E.; Shafiee, A.; Jandaghi, A. B.; Doostmohammadi, A.; Fathi, M. H.; Farhadian, S.; Soleimani, M. *ACS Appl. Mater. Interfaces* **2011**, *3*, 4518−4524.
(18) Yanagida, H.; Okada, M.; Masuda, M.; Narama, I.; Nakano, S.; Kitao, S.; Takakuda, K.; Furuzono, T. *J. Artif. Organs* **2011**, *14*, 331−341.
(19) Jegal, S. H.; Park, J. H.; Kim, J. H.; Kim, T. H.; Shin, U. S.; Kim, T. I.; Kim, H. W. *Acta Biomater.* **2011**, *7*, 1609−1617.
(20) Fu, S.; Ni, P.; Wang, B.; Chu, B.; Peng, J.; Zheng, L.; Zhao, X.; Luo, F.; Wei, Y.; Qian, Z. *Biomaterials* **2012**, *33*, 8363−8371.
(21) Spadaccio, C.; Rainer, A.; Trombetta, M.; Vadala, G.; Chello, M.; Covino, E.; Denaro, V.; Toyoda, Y.; Genovese, J. A. *Ann. Biomed. Eng.* **2009**, *37*, 1376−1389.
(22) Yim, E. K.; Pang, S. W.; Leong, K. W. *Exp. Cell Res.* **2007**, *313*, 1820−1829.
(23) Chevallier, N.; Anagnostou, F.; Zilber, S.; Bodivit, G.; Maurin, S.; Barrault, A.; Bierling, P.; Hernigou, P.; Layrolle, P.; Rouard, H. *Biomaterials* **2010**, *31*, 270−278.
(24) Kilian, K. A.; Bugarija, B.; Lahn, B. T.; Mrksich, M. *Proc. Natl. Acad. Sci. U.S.A.* **2010**, *107*, 4872−4877.
(25) McBeath, R.; Pirone, D. M.; Nelson, C. M.; Bhadriraju, K.; Chen, C. S. *Dev. Cell* **2004**, *6*, 483−495.
(26) Dalby, M. J.; Gadegaard, N.; Tare, R.; Andar, A.; Riehle, M. O.; Herzyk, P.; Wilkinson, C. D. W.; Oreffo, R. O. C. *Nat. Mater.* **2007**, *6*, 997−1003.
(27) Engler, A. J.; Sen, S.; Sweeney, H. L.; Discher, D. E. *Cell* **2006**, *126*, 677−689.
(28) Oh, S.; Brammer, K. S.; Li, Y. S. J.; Teng, D.; Engler, A. J.; Chien, S.; Jin, S. *Proc. Natl. Acad. Sci. U.S.A.* **2009**, *106*, 2130−2135.
(29) Parekh, S. H.; Chatterjee, K.; Lin-Gibson, S.; Moore, N. M.; Cicerone, M. T.; Young, M. F.; Simon, C. G. *Biomaterials* **2011**, *32*, 2256−2264.
(30) Kim, S. S.; Sun Park, M.; Jeon, O.; Yong Choi, C.; Kim, B. S. *Biomaterials* **2006**, *27*, 1399−1409.
(31) Park, K. H.; Na, K.; Kim, S. W.; Sun, B. K.; Woo, D. G.; Yang, H. N.; Chung, H. M. *Biomaterials* **2007**, *28*, 2631−2637.
(32) Tsiridis, E.; Bhalla, A.; Zubier, A.; Gurav, N.; Heliotis, M.; Deb, S.; DiSilvio, L. *Injury* **2006**, *37*, S25−S32.
(33) McCabe, L. R.; Shu, R.; McMullen, R.; Baumann, M. J. *J. Biomed. Mater. Res. A* **2003**, *67A*, 1196−1204.
(34) Lin, L.; Chow, K. L.; Leng, Y. *J. Biomed. Mater. Res. A* **2009**, *89*, 326−335.
(35) Polini, A.; Pisignano, D.; Parodi, M.; Quarto, R.; Scaglione, S. *Plos One* **2011**, *6*, e26211.
(36) Lü, L. X.; Wang, Y. Y.; Mao, X.; Xiao, Z. D.; Huang, N. P. *Biomed Mater* **2012**, *7*, 015002.
(37) Mao, X.; Chu, C. L.; Mao, Z.; Wang, J. J. *Tissue Cell* **2005**, *37*, 349−357.
(38) Wang, Y. Y.; Lü, L. X.; Shi, J. C.; Wang, H. F.; Xiao, Z. D.; Huang, N. P. *Biomacromolecules* **2011**, *12*, 551−559.
(39) Wang, Y. Y.; Lü, L. X.; Feng, Z. Q.; Xiao, Z. D.; Huang, N. P. *Biomed. Mater.* **2010**, *5*, 054112.
(40) Tian, T.; Wang, Y. Y.; Wang, H. T.; Zhu, Z. Q.; Xiao, Z. D. *J. Cell Biochem.* **2010**, *111*, 488−496.
(41) Livak, K. J.; Schmittgen, T. D. *Methods* **2001**, *25*, 402−408.
(42) Schmitz, J. P.; Hollinger, J. O. *Clin. Orthop. Relat. Res.* **1986**, *205*, 299−308.
(43) Hedberg, E. L.; Kroese-Deutman, H. C.; Shih, C. K.; Crowther, R. S.; Carney, D. H.; Mikos, A. G.; Jansen, J. A. *Biomaterials* **2005**, *26*, 4616−4623.
(44) Tu, J.; Wang, H.; Li, H.; Dai, K.; Wang, J.; Zhang, X. *Biomaterials* **2009**, *30*, 4369−4376.
(45) Liu, Y.; Lu, Y.; Tian, X.; Cui, G.; Zhao, Y.; Yang, Q.; Yu, S.; Xing, G.; Zhang, B. *Biomaterials* **2009**, *30*, 6276−6285.
(46) Jang, J. H.; Castano, O.; Kim, H. W. *Adv. Drug Deliver Rev.* **2009**, *61*, 1065−1083.
(47) Murugan, R.; Ramakrishna, S. *Compos. Sci. Technol.* **2005**, *65*, 2385−2406.
(48) Stevens, M. M.; George, J. H. *Science* **2005**, *310*, 1135−1138.
(49) Peng, F.; Yu, X.; Wei, M. *Acta Biomater.* **2011**, *7*, 2585−2592.
(50) Smith, I. O.; McCabe, L. R.; Baumann, M. J. *Int. J. Nanomed.* **2006**, *1*, 189−194.

(51) Rouahi, M.; Champion, E.; Hardouin, P.; Anselme, K. *Biomaterials* **2006**, *27*, 2829−2844.
(52) Zhou, G. S.; Su, Z. Y.; Cai, Y. R.; Liu, Y. K.; Dai, L. C.; Tang, R. K.; Zhang, M. *Biomed. Mater. Eng.* **2007**, *17*, 387−395.
(53) Kim, K.; Dean, D.; Lu, A.; Mikos, A. G.; Fisher, J. P. *Acta Biomater.* **2011**, *7*, 1249−1264.
(54) Ripamonti, U. *Biomaterials* **1996**, *17*, 31−35.
(55) Yin, Z.; Chen, X.; Chen, J. L.; Shen, W. L.; Hieu Nguyen, T. M.; Gao, L.; Ouyang, H. W. *Biomaterials* **2010**, *31*, 2163−2175.